ONLINE DATA SUPPLEMENT

Conflicting physiological and genomic cardiopulmonary effects of recruitment maneuvers in murine acute lung injury

Armand Mekontso Dessap, Guillaume Voiriot, Tong Zhou, Elisabeth Marcos, Steven M Dudek, Jeff R Jacobson, Roberto Machado, Serge Adnot, Laurent Brochard, Bernard Maitre, and Joe GN Garcia

MATERIAL AND METHODS

Animal protocol

The experiments were performed in accordance with the official regulations of the French Ministry of Agriculture and the US National Institute of Health guidelines for the experimental use of animals. Male C57BL/6 mice weighing 20 to 30 g were anesthetized with inhaled 5% isoflurane (Abbott, Rungis, France), and suspended by their upper incisors from a rubber band on a 60° incline board. The tongue was gently extended to prevent swallowing, and a 50 µL volume instillate (consisting of PBS or 4 µg/g of E. coli LPS, O55:B5, Sigma-Aldrich Chimie, Lyon, France) was delivered into the distal part of the oropharynx and aspirated into the lower respiratory tract (E1). After oropharyngeal aspiration, the mice returned to their cages for 18 hours, then were reanesthetized with intraperitoneal pentobarbital (30 µg/g of body weight, Hospira, Meudon La Forêt, France) followed by continuous 5% isoflurane (Abbott, Rungis, France). The larynx was surgically exposed and the trachea was intubated orally under direct vision with a metal cannula (internal diameter of 1 mm, Harvard Apparatus, Les Ulis, France).

The tracheal cannula was properly secured with surgical thread (Ethicon 3-0, Ethicon, Auneau, France) before connection to mechanical ventilator in order to avoid leaks.

Mechanical ventilation

Mice were ventilated in the supine position using humidified gas (20 mgH_2O/L absolute humidity, MR410 humidifier, Fischer & Paykel Healthcare, Courtaboeuf, France), with a tidal volume of 8 µL/g of body weight, a respiratory rate of 180/min, 3 cmH_2O end-expiratory pressure, and FiO_2 of 1, by means of a computer-driven small-animal ventilator (*flexiVent*, Scireq, Montreal, Canada). Because load impedance has been shown to influence ventilator performance and the resulting delivered tidal volume (E2), the displacement volume of the piston was manually adjusted on a regular basis to make sure that the delivered tidal volume was 8 µL/g of body weight. Mechanical ventilation lasted 5 hours with continuous anesthesia maintained by 1% isoflurane and muscle paralysis using intraperitoneal pancuronium at the onset of the experiment and every two hours (0.8 µL/g of body weight, Organon, Puteaux, France) to ensure passive mechanical conditions. The body temperature was monitored using a rectal probe and was maintained at 36.5 °C with a blanket connected to a homeothermic regulator (Homeo-blanket system 50-7221F, Harvard Apparatus, Les Ulis, France). Mice received intraperitoneal warm fluid boluses (5% dextrose with 9 g/L NaCl) at the onset of the experiment (20 µL/g of body weight) and every hour (10 µL/g of body weight).

Experimental design

The experimental design included four groups: PBS+TI (PBS aspiration followed by mechanical ventilation with tidal inflations only), PBS+DI (PBS aspiration followed by mechanical ventilation with intermittent DI), LPS+TI (LPS aspiration followed by mechanical ventilation

with tidal inflations only), and LPS+DI (LPS aspiration followed by mechanical ventilation with intermittent DI). DI maneuvers were delivered by the *flexiVent* ventilator in a quasi-sinusoidal, nonsustained, and nonpressure-limited fashion in order to mimic the tidal inflations. A volume of 0.75 mL delivered twice per minute was chosen as this recruitment strategy was previously shown to safely improve lung mechanics during a 2 hour ventilation protocol in a murine model while conferring protection from biotrauma (E3).

Respiratory mechanics

Special features of the *flexiVent* ventilator include a continuous monitoring of airway pressures and a precision computer-controlled piston that is capable of accurately measuring the delivered volume (with appropriate corrections for gas compression) and to produce any desired waveform, allowing respiratory mechanics assessment with the forced oscillation technique (FOT) and pressure-volume curves (E3). Before each mouse was connected to the ventilator, pressure and piston displacement calibration data were collected to correct the respiratory mechanics data (E4). Mice were allowed to stabilize on the ventilator for 5 minutes and were then inflated three times to a transrespiratory pressure of 30 cmH_2O to establish a standard volume history. FOT were assessed at initiation of mechanical ventilation (before and after volume history standardization), and then repeated hourly to capture the time course and the detailed response to mechanical ventilation. FOT measurements included a 1.2 second, 2.5 Hz single-frequency signal (SnapShot-150 perturbation) and an eight seconds, broadband low-frequency signal containing 17 mutually prime frequencies between 0.5 and 19.75 Hz (Quick Prime-8 perturbation). Respiratory system dynamic resistance, elastance, and compliance were calculated in the *flexiVent* software by fitting the single frequency FOT data to the single compartment model (E5). Respiratory system input impedance was calculated from the low frequency FOT data and

airway Newtonian resistance, tissue damping and tissue elastance were determined by iteratively fitting the constant-phase model to input impedance (E6). In addition, a continuous pressure-volume curve (pressure-driven from 3 to 30 cmH_2O) was performed at start and end of mechanical ventilation. The loops were processed by the *flexiVent* software to fit the Salazar-Knowles equation and to calculate parametric results, such as the quasi-static compliance of the respiratory system. Before the end of the timed ventilator protocol, mice underwent hemodynamic explorations.

Hemodynamic explorations

Through the cervical midline incision, both the right jugular vein and left carotid artery were isolated using a stereomicroscope (Leica MZ 7.5, Leica Microsystems, Nanterre, France). An ultra-miniature 1.4F high fidelity pressure transducer catheter (SPR-671, Millar Instruments, Houston, TX) was inserted into the right jugular vein and advanced into the right ventricle. The micromanometer was calibrated in vitro electronically and against a column of mercury with the reference zero level taken at midchest. Right ventricular systolic pressure was measured during a short respiratory pause with the use of a Gould transducer (Gould, Cleveland, USA) and a Notocord system (Emka Technologies, Paris, France). Cardiac output was measured by the transpulmonary thermodilution technique (E7). Briefly, a thermistor microprobe (Fr-1; Columbus Instruments, Columbus, OH) was inserted into the left carotid artery and advanced to the aortic arch, where changes in aortic blood temperature were measured. A catheter placed in the right jugular vein was advanced to the right atrium for rapid bolus injection of 20 µL of saline solution at 20°C with the use of a constant rate syringe (Hamilton Company, Reno, NV). Cardiac output was computed in triplicate and averaged, using the Cardiomax-III system (Columbus

Instruments). Total pulmonary vascular resistances were calculated as the ratio of right ventricular systolic pressure to cardiac output.

Specimen collection

At the end of the timed ventilator protocol and after hemodynamic measurements, arterial blood was obtained via carotid puncture, using a heparinized needle and syringe, for determination of blood gases using a GEM Premier 3000 analyser (Instrumentation Laboratory, Lexington, MA, USA) and subsequent measurement of cytokines, chemokines and markers of endothelial injury using Bioplex (Bio-Rad, Hercules, CA) and Milliplex (Millipore Corporation, Billerica, MA) mouse multi-analyte cytokine kits in accordance with manufacturer's instructions. Immediately following thoracotomy, the heart was removed and right and left ventricles were carefully isolated by manual dissection, then immediately quick-frozen in liquid nitrogen and stored at -80°C. The right lower bronchus was sutured, and the right lower lobe of the lung was removed, quick-frozen in liquid nitrogen and stored at -80°C. The remaining lung was lavaged with four separate 0.5 mL aliquots of saline at 20°C and then underwent fixation (4% paraformaldehyde) and paraffin embedding.

Bronchoalveolar lavage

The total cell count was determined for a fresh fluid specimen using a Malassez hemocytometer. The cell pellet was diluted in saline, and differential cell counts were done on cytocentrifuge preparations in few animals (Cytospin 3; Shandon Scientific, Cheshire, UK) stained with Diff-Quick stain (Baxter Diagnostics, McGaw Park, IL). Bronchoalveolar lavage fluid was centrifuged (1600 rpm, 7 min at 4°C), and cell-free supernatants were stored at –80°C for subsequent assessment of protein content (using a colorimetric BCA assay, Thermo Scientific,

Rockford, IL), and cytokines and chemokines concentrations (using a multi-analyte Bioplex mouse cytokine kit, Bio-Rad, Hercules, CA) in accordance with manufacturer's instructions.

Histological analysis

Lung sections of 5 μm thickness were cut and stained with hematoxylin and eosin. True color high resolution digital images were obtained from stained slides using an Aperio ScanScope CS scanner (Aperio, Vista, CA) with a 20× scanning magnification. The degree of lung injury was blindly determined using a high speed automated whole-slide quantitative image analysis tool (Genie histology pattern recognition, ImageScope version 6.25 software, Aperio, Vista, CA) (E8). Briefly, the Genie software was trained to recognize different components of lung structure (conducting airways, blood vessels, and lung parenchyma). Then positive pixel counts and colocalization scoring algorithms were used to identify different elements within these components (air, proteinaceous fluid/hyalines membranes, and cells). After successful training, quantitative image analysis tools were used to automatically assess the following parameters on entire lung tissue sections across a large set of slides (n=9 to 12 animals per group): lung edema (defined as the relative surface occupied by fluid/hyaline membranes within lung parenchyma); and vascular congestion (defined as the relative surface occupied by cells within vessels).

RNA isolation and transcript analysis

We extracted total RNA from frozen tissues with a combined protocol using TRIzol reagent (Invitrogen, Carlsbad, CA) and the RNeasy kit (Qiagen, Valencia, CA) as previously described (E9, 10). For each group, we prepared RNA from the tissues of three to four animals. We used total RNA (5 μg) to synthesize double-stranded cDNA using the One-Cycle cDNA Synthesis Kit (Affymetrix, Santa Clara, CA). The cDNA served as a template to synthesize biotin-labeled

antisense cRNA using an IVT Labeling Kit (Affymetrix). Labeled cRNA was fragmented and hybridized to the Affymetrix Mouse Genome 430 2.0 Array (containing ~ 34,000 genes), as described in the Affymetrix GeneChip protocol. Chips were scanned using a GeneChip Scanner 3000 (Affymetrix).

Oligonucleotide array analysis

We evaluated chip quality, including RNA degradation, reverse transcription, cRNA synthesis and labeling, hybridization, chip washing, and scanning, using GCOS, dChip, and the Bioconductor Affy package (E11, 12). Arrays were normalized and processed using Bioconductor "GCRMA" package. To identify differentially expressed genes, we conducted pairwise comparisons using Significance Analysis of Microarrays (E13). For probe sets representing the same Entrez Gene [National Center for Biotechnology Information (NCBI) 2008a] or UniGene accession numbers (NCBI 2008c), we included only the probe set with the lowest false detection rate in the gene list. *The microarray data have been submitted to the NCBI's Gene Expression Omnibus Datasets.*

Identification of gene ontology categories and pathways enriched with dysregulated genes.

The lists of dysregulated genes were imported into DAVID (Database for Annotation, Visualization and Integrated Discovery, http://david.abcc.ncifcrf.gov/) (E14). The genes in these lists were mapped to DAVID identifiers, and then functionally annotated using the DAVID default gene ontology categories (biological processes, cellular components, molecular functions) and pathways [BBID (Biological Biochemical Image Database), KEGG (Kyoto Encyclopedia of Genes and Genomes**)**, and Biocarta]. The number of genes in each functional classification category was compared against that of all genes in the Affymetrix Mouse Genome 430 2.0 Array

(modified Fisher Exact test), to determine the significance of the category or pathway. Due to the redundant nature of annotations, we used the functional annotation clustering algorithm, which integrates Kappa statistics and fuzzy heuristic clustering to group annotations with common gene members together. The group enrichment score, calculated as the geometric mean (in log scale) of member's p-values in a corresponding cluster, was used to rank cluster's biological significance.

Quantitative RT-PCR. Quantification of selected transcripts was performed by TaqMan real-time RT-PCR assays using a CFX384 Rea-Time PCR Detection System (Biorad, Hercules, CA). cDNAs were generated from 1 μg of total RNA using the qScript cDNA SuperMix kit (Quanta BioSciences, Gaithersburg, MD). The resulting cDNA was subjected to a 40 cycles PCR amplification using manufacturer's TaqMan Gene Expression Master Mix Kit protocol. The ready-made primer and probe sets were ordered from *Applied Biosystems.* (Catalog #: Il6: Mm01210733_m1; Cxcl1: Mm00433859_m1; Sele: Mm01310199_m1; Tnc: Mm00495681_m1; Edn1: Mm00438659_m1; Angpt1: Mm00456503_m1; Dio2: Mm00515664_m1; Rnd1: Mm01310221_m1; Bmp4: Mm00432087_m1; Scube2: Mm01166099_m1; Actb: 4352933E; Angpt2: Mm00545826_m1; Procr: Mm00440992_m1; Adamts4: Mm01295275_m1; Thbs1: Mm01335418_m1). Three replicates were run for each gene for each sample in a 384- well plate. Actin-b was used as the endogenous reference gene as it did not exhibit significant expression changes between groups. The relative quantitation method (ΔΔCt) was used, with the ratio of the mRNA level for the gene of interest normalized to the level of endogenous reference gene and the average of the PBS+TI samples as the calibrator value.

REFERENCES

E1. Foster WM, Walters DM, Longphre M, Macri K, Miller LM. Methodology for the measurement of mucociliary function in the mouse by scintigraphy. J Appl Physiol 2001;90(3):1111-1117.

E2. Thammanomai A, Majumdar A, Bartolak-Suki E, Suki B. Effects of reduced tidal volume ventilation on pulmonary function in mice before and after acute lung injury. J Appl Physiol 2007;103(5):1551-1559.

3. Allen GB, Suratt BT, Rinaldi L, Petty JM, Bates JH. Choosing the frequency of deep inflation in mice: Balancing recruitment against ventilator-induced lung injury. Am J Physiol Lung Cell Mol Physiol 2006;291(4):L710-717.

E4. Schuessler TF, Bates JH. A computer-controlled research ventilator for small animals: Design and evaluation. IEEE Trans Biomed Eng 1995;42(9):860-866.

5. Pillow JJ, Korfhagen TR, Ikegami M, Sly PD. Overexpression of tgf-alpha increases lung tissue hysteresivity in transgenic mice. J Appl Physiol 2001;91(6):2730-2734.

E6. Hantos Z, Daroczy B, Suki B, Nagy S, Fredberg JJ. Input impedance and peripheral inhomogeneity of dog lungs. J Appl Physiol 1992;72(1):168-178.

E7. Champion HC, Villnave DJ, Tower A, Kadowitz PJ, Hyman AL. A novel right-heart catheterization technique for in vivo measurement of vascular responses in lungs of intact mice. Am J Physiol Heart Circ Physiol 2000;278(1):H8-H15.

E8. Gilbertson JR, Ho J, Anthony L, Jukic DM, Yagi Y, Parwani AV. Primary histologic diagnosis using automated whole slide imaging: A validation study. BMC Clin Pathol 2006;6:4.

E9. Hong SB, Huang Y, Moreno-Vinasco L, Sammani S, Moitra J, Barnard JW, Ma SF, Mirzapoiazova T, Evenoski C, Reeves RR, Chiang ET, Lang GD, Husain AN, Dudek SM, Jacobson JR, Ye SQ, Lussier YA, Garcia JG. Essential role of pre-b-cell colony enhancing factor in ventilator-induced lung injury. Am J Respir Crit Care Med 2008;178(6):605-617.

E10. Meyer NJ, Huang Y, Singleton PA, Sammani S, Moitra J, Evenoski CL, Husain AN, Mitra S, Moreno-Vinasco L, Jacobson JR, Lussier YA, Garcia JG. Gadd45a is a novel candidate gene in inflammatory lung injury via influences on akt signaling. Faseb J 2009;23(5):1325-1337.

E11. Li C, Hung Wong W. Model-based analysis of oligonucleotide arrays: Model validation, design issues and standard error application. Genome Biol 2001;2(8):RESEARCH0032.

E12. Bolstad BM, Irizarry RA, Astrand M, Speed TP. A comparison of normalization methods for high density oligonucleotide array data based on variance and bias. Bioinformatics 2003;19(2):185-193.

E13. Tusher VG, Tibshirani R, Chu G. Significance analysis of microarrays applied to the ionizing radiation response. Proc Natl Acad Sci U S A 2001;98(9):5116-5121.

E14. Huang da W, Sherman BT, Lempicki RA. Systematic and integrative analysis of large gene lists using david bioinformatics resources. Nat Protoc 2009;4(1):44-57.

FIGURE LEGENDS

Figure E1. Genes involved in lung vascular processes that are dysregulated by LPS+DI challenge but not LPS+TI. Groups were compared using significance analysis of microarray (LPS+DI vs. PBS+TI and LPS+TI vs. PBS+TI) and the lists of dysregulated genes were explored by DAVID functional annotation clustering to assess significance of gene-term enrichment. Involvement or not of a given gene in the corresponding gene ontology category are highlighted in green and black respectively. A=GO:0001525~angiogenesis, B=GO:0048514~blood vessel morphogenesis, C=GO:0001568~blood vessel development, D=GO:0001944~vasculature development.

Figure E2. KEGG (Kyoto Encyclopedia of Genes and Genomes) pathway map of vascular smooth muscle contraction. Red stars indicate genes dysregulated in lungs from LPS+DI group but not LPS+TI group (using PBS+TI as the reference group). PBS, phosphate buffered saline aspiration; LPS, lipopolysaccharide aspiration. TI, ventilation with tidal inflations only, DI, ventilation with deep inflations.

Figure E3. Top 10 right ventricular clusters of gene ontologies and pathways enriched by LPS+DI. Groups were compared using significance analysis of microarray (LPS+DI vs. PBS+TI and LPS+TI vs. PBS+TI) and the lists of dysregulated genes were explored by DAVID functional annotation clustering to assess significance of gene-term enrichment. Bars represent the log transformed enrichment p value (modified Fischer's exact test) of each category for the LPS+DI vs. PBS+TI comparison (dark grey) and for the LPS+TI vs. PBS+TI comparison (light grey). Clusters are ranked according to their enrichment score (calculated as the geometric mean of the

enrichment p values of all categories within the cluster) for the LPS+DI vs. PBS+TI comparison. The vertical dashed line represents the 0.05 significance threshold. TI, ventilation with tidal inflations only, DI, ventilation with deep inflations; PBS, phosphate buffered saline aspiration; LPS, lipopolysaccharide aspiration.

Figure E4. Top 10 left ventricular clusters of gene ontologies and pathways enriched by LPS+TI. Groups were compared using significance analysis of microarray (LPS+TI vs. PBS+TI and PBS+DI vs. PBS+TI) and the lists of dysregulated genes were explored by DAVID functional annotation clustering to assess significance of gene-term enrichment. Bars represent the log transformed enrichment p value (modified Fischer's exact test) of each category for the LPS+TI vs. PBS+TI comparison (dark grey) and for the PBS+DI vs. PBS+TI comparison (light grey). The top 10 clusters are those with the highest enrichment score (calculated as the geometric mean of the enrichment p values of all categories within the cluster) for the LPS+TI vs. PBS+TI comparison. The vertical dashed line represents the 0.05 significance threshold. PBS, phosphate buffered saline aspiration; LPS, lipopolysaccharide aspiration; TI, ventilation with tidal inflations only, DI, ventilation with deep inflations.

Figure E5. Absolute concentrations of various cytokines, chemokines and endothelium markers in bronchoalveolar lavage (panel A) and plasma (panel B) by multi-analyte assay for PBS+TI (green), PBS+DI (striped green), LPS+TI (red), and LPS+DI (striped red). PBS, phosphate buffered saline aspiration; LPS, lipopolysaccharide aspiration; TI, ventilation with tidal inflations only, DI, ventilation with deep inflations.

SUPPLEMENTAL TABLES AND FIGURES

Table E1. Gene filtering criteria and results of lung and heart microarray analysis by significant analysis of microarray

			Number of dysregulated unique genes		
	False discovery rate	Fold change	PBS+DI vs. PBS+TI	LPS+TI vs. PBS+TI	LPS+DI vs. PBS+TI
Lung	5%	2	0	660 (334 up / 326 down)	1697 (710 up / 987 down)
Right ventricle	10%	2	0	431 (17 up / 414 down)	188 (64 up / 124 down)
Left ventricle	10%	2	155 (1 up / 154 down)	1276 (460 up / 816 down)	539 (326 up / 21 down)

PBS, phosphate buffered saline aspiration; LPS, lipopolysaccharide aspiration; TI, ventilation with tidal inflations only, DI, ventilation with deep inflations.

Figure E1.


ephrin B2
matrix metallopeptidase 2
suppressor of cytokine signaling 3
collagen, type III, alpha 1
sphingosine kinase 1
reversion-inducing-cysteine-rich protein with kazal motifs; similar to Reversion-inducing cysteine-rich protein with Kazal motifs precurs
polycystic kidney disease 1 homolog
histone deacetylase 7; similar to histone deacetylase 7A
paired related homeobox 1
myocyte enhancer factor 2C
MAD homolog 7 (Drosophila)
caveolin 1, caveolae protein
zinc finger protein, multitype 2
predicted gene 4066; smoothened homolog (Drosophila)
transglutaminase 2, C polypeptide
similar to Wilms tumor homolog; Wilms tumor 1 homolog
similar to Quaking protein; quaking
heparin-binding EGF-like growth factor
nitric oxide synthase 3, endothelial cell
SRY-box containing gene 17
endothelin 1
angiopoietin 2
neuropilin 1
fibroblast growth factor 1
SRY-box containing gene 18
angiogenin, ribonuclease, RNase A family, 5
heme oxygenase (decycling) 1
interleukin 1 beta
Meis homeobox 1
sonic hedgehog
hypoxia inducible factor 1, alpha subunit
chondroitin sulfate proteoglycan 4
sema domain, seven thrombospondin repeats (type 1 and type 1-like), transmembrane domain (TM) and short cytoplasmic domain, (s
tumor necrosis factor, alpha-induced protein 2
ELK3, member of ETS oncogene family
matrix metallopeptidase 19
Rho GTPase activating protein 24
kinase insert domain protein receptor
cysteine rich protein 61
epiregulin
mesenchyme homeobox 2
A B C D

Figure E2.

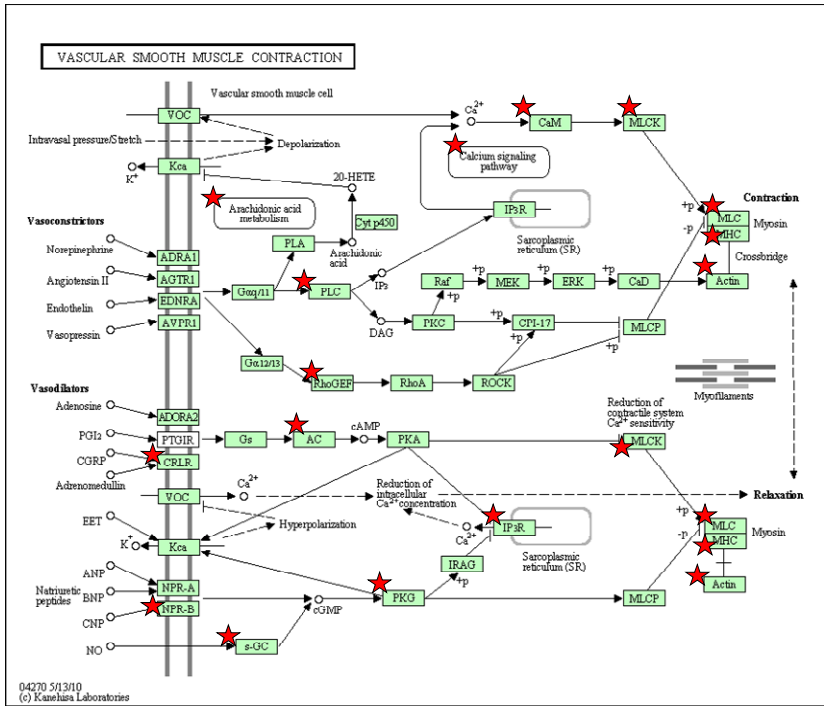
VASCULAR SMOOTH MUSCLE CONTRACTION
Vascular smooth muscle cell
VOC
Intravasal pressure/Stretch
Depolarization
Kca
20-HETE
Arachidonic acid metabolism
Cyt p450
Vasoconstrictors
Norepinephrine
Angiotensin II
Endothelin
Vasopressin
ADRA1
AGTR1
EDNRA
AVPR1
PLA
Arachidonic acid
Gαq/11
PLC
IPs
DAG
Gα12/13
RhoGEF
RhoA
ROCK
PKC
Raf
MEK
ERK
CaD
CPI-17
MLCP
Ca2+
CaM
MLCK
Calcium signaling pathway
IPsR
Sarcoplasmic reticulum (SR)
Contraction
MLC
MHC
Myosin
Crossbridge
Actin
Myofilaments
Vasodilators
Adenosine
PGI2
CGRP
Adrenomedullin
ADORA2
PTGIR
CRLR
Gs
AC
cAMP
PKA
Reduction of contractile system Ca2+ sensitivity
Reduction of intracellular Ca2+ concentration
Hyperpolarization
Relaxation
EET
ANP
Natriuretic peptides
BNP
CNP
NO
NPR-A
NPR-B
s-GC
cGMP
PKG
IRAG
04270 5/13/10
(c) Kanehisa Laboratories

Figure E3.

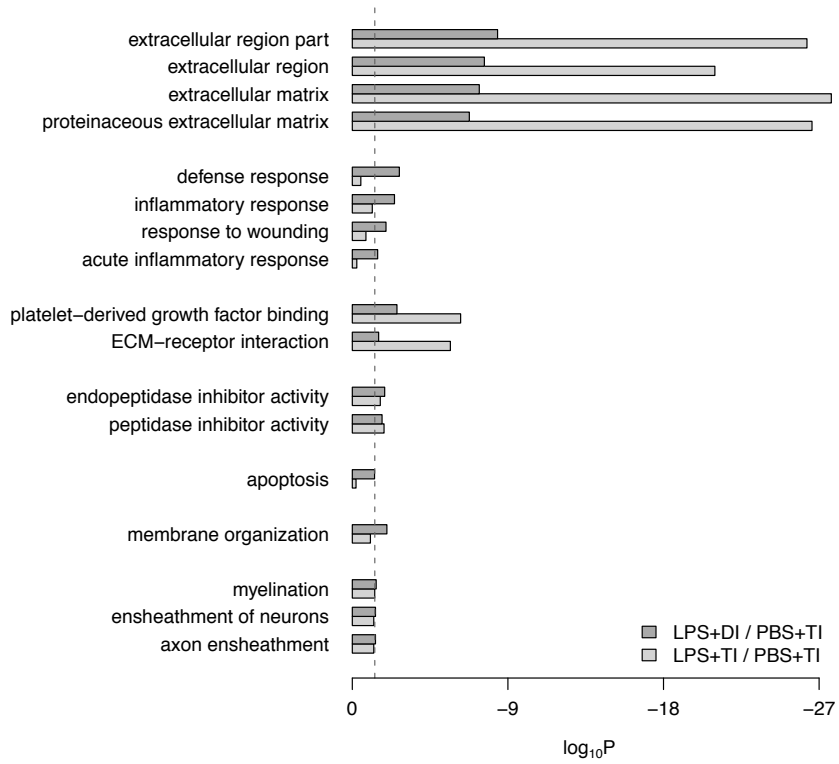
extracellular region part
extracellular region
extracellular matrix
proteinaceous extracellular matrix
defense response
inflammatory response
response to wounding
acute inflammatory response
platelet−derived growth factor binding
ECM−receptor interaction
endopeptidase inhibitor activity
peptidase inhibitor activity
apoptosis
membrane organization
myelination
ensheathment of neurons
axon ensheathment
LPS+DI / PBS+TI
LPS+TI / PBS+TI
0
−9
−18
−27
log10P

Figure E4.

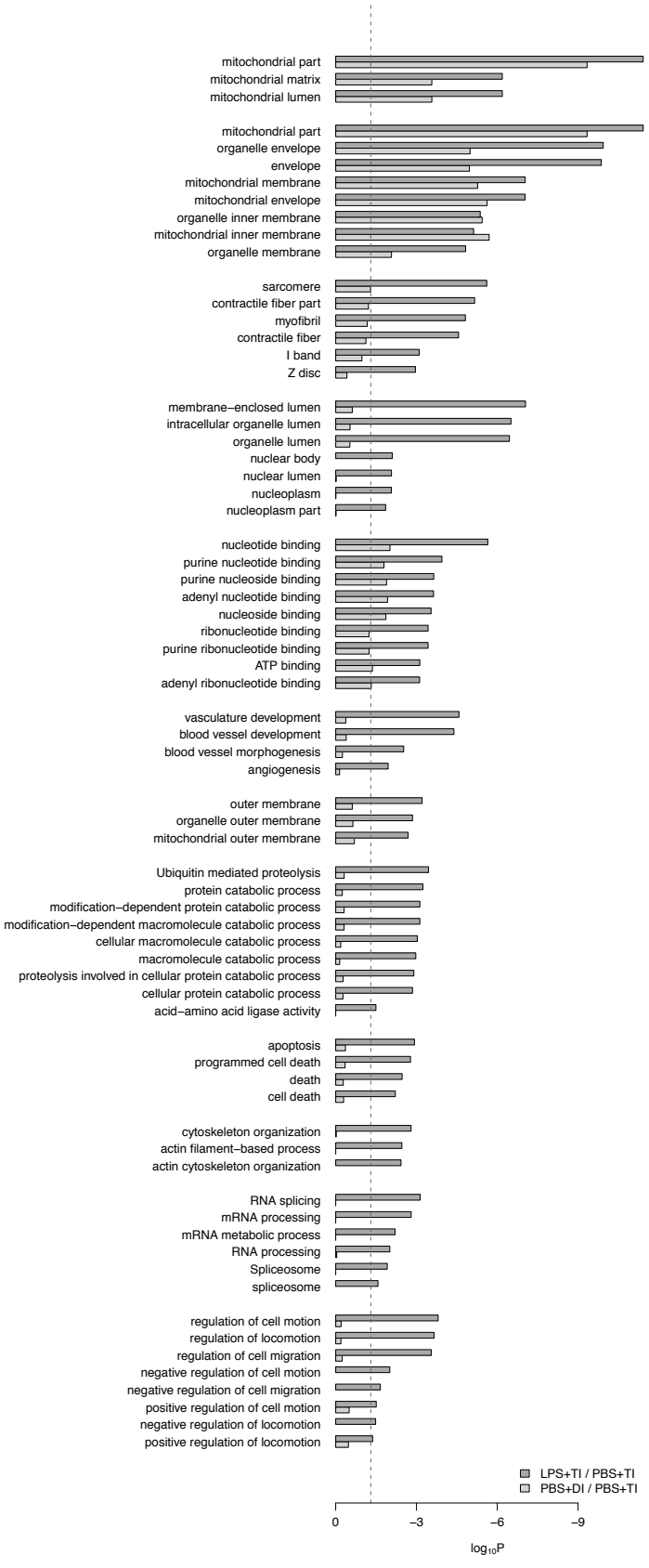
mitochondrial part
mitochondrial matrix
mitochondrial lumen
mitochondrial part
organelle envelope
envelope
mitochondrial membrane
mitochondrial envelope
organelle inner membrane
mitochondrial inner membrane
organelle membrane
sarcomere
contractile fiber part
myofibril
contractile fiber
I band
Z disc
membrane−enclosed lumen
intracellular organelle lumen
organelle lumen
nuclear body
nuclear lumen
nucleoplasm
nucleoplasm part
nucleotide binding
purine nucleotide binding
purine nucleoside binding
adenyl nucleotide binding
nucleoside binding
ribonucleotide binding
purine ribonucleotide binding
ATP binding
adenyl ribonucleotide binding
vasculature development
blood vessel development
blood vessel morphogenesis
angiogenesis
outer membrane
organelle outer membrane
mitochondrial outer membrane
Ubiquitin mediated proteolysis
protein catabolic process
modification−dependent protein catabolic process
modification−dependent macromolecule catabolic process
cellular macromolecule catabolic process
macromolecule catabolic process
proteolysis involved in cellular protein catabolic process
cellular protein catabolic process
acid−amino acid ligase activity
apoptosis
programmed cell death
death
cell death
cytoskeleton organization
actin filament−based process
actin cytoskeleton organization
RNA splicing
mRNA processing
mRNA metabolic process
RNA processing
Spliceosome
spliceosome
regulation of cell motion
regulation of locomotion
regulation of cell migration
negative regulation of cell motion
negative regulation of cell migration
positive regulation of cell motion
negative regulation of locomotion
positive regulation of locomotion
LPS+TI / PBS+TI
PBS+DI / PBS+TI
0
−3
−6
−9
log10P

Figure E5

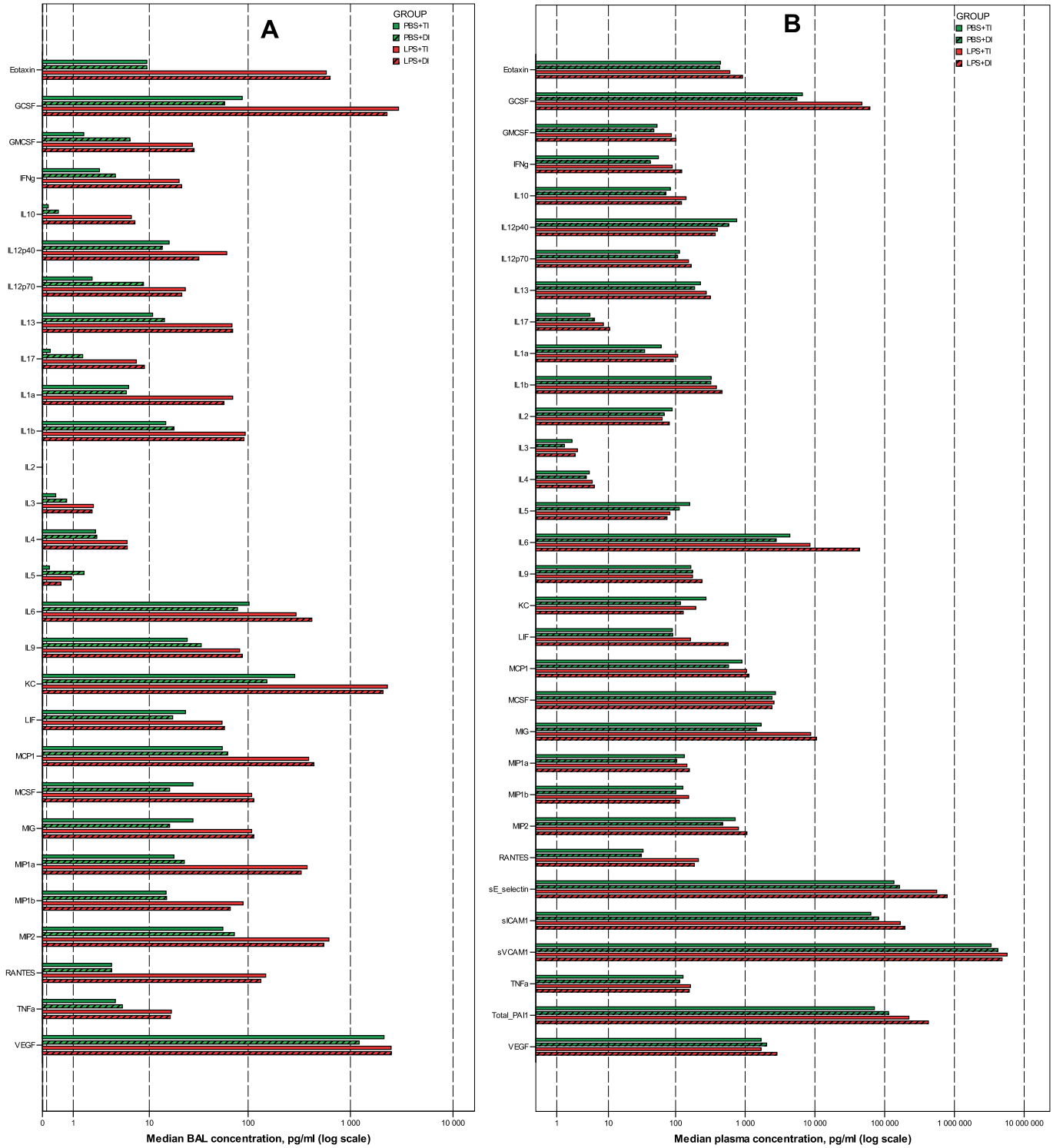
A
GROUP
PBS+TI
PBS+DI
LPS+TI
LPS+DI
Eotaxin
GCSF
GMCSF
IFNg
IL10
IL12p40
IL12p70
IL13
IL17
IL1a
IL1b
IL2
IL3
IL4
IL5
IL6
IL9
KC
LIF
MCP1
MCSF
MIG
MIP1a
MIP1b
MIP2
RANTES
TNFa
VEGF
0
1
10
100
1 000
10 000
Median BAL concentration, pg/ml (log scale)
B
GROUP
PBS+TI
PBS+DI
LPS+TI
LPS+DI
Eotaxin
GCSF
GMCSF
IFNg
IL10
IL12p40
IL12p70
IL13
IL17
IL1a
IL1b
IL2
IL3
IL4
IL5
IL6
IL9
KC
LIF
MCP1
MCSF
MIG
MIP1a
MIP1b
MIP2
RANTES
sE_selectin
sICAM1
sVCAM1
TNFa
Total_PAI1
VEGF
1
10
100
1 000
10 000
100 000
1 000 000
10 000 000
Median plasma concentration, pg/ml (log scale)